Available on CMS information server

CMS CR -2024/348

The Compact Muon Solenoid Experiment

Conference Report

Mailing address: CMS CERN, CH-1211 GENEVA 23, Switzerland

17 December 2024 (v3, 21 January 2025)

Gas gaps and chambers quality control of improved resistive plate chambers (iRPC)

Mohammad Ahammad Ali on behalf of CMS Collaboration

Abstract

In preparation for the Phase-II upgrade for the High-Luminosity LHC program, 72 improved Resistive Plate Chambers (iRPC) will be installed in the third and fourth endcap disks of the Compact Muon Solenoid detector during the annual technical stop 2024. This new generation of RPC detectors will operate in a low-angle momentum (extending RPC coverage from pseudorapidity $|\eta|$ = 1.9 to 2.4), in a high radiation environment, and will bring a better space and time resolution for this challenging region. To ensure proper performance, iRPC chambers undergo a series of quality control (QC) tests at each stage of the assembly chain. These tests include QC1 for the basic components, QC2 for chamber elements such as gaps and cooling, QC3 for evaluating the full chamber performance after production, which includes noise, efficiency, current, lastly QC4 for the final validation of the chambers. In this work we present the different QC stages and discuss test results for the newly built iRPCs at the assembly sites.

Presented at *RPC2024 XVII International Conference on Resistive Plate Chambers and Related Detectors (RPC2024)*

Gas gaps and chambers quality control of improved Resistive Plate Chambers

M. A. Ali [ah], B. El-Mahdy [l,1], F.E. Neri Huerta [ad], M. Tytgat [a,2], K. Mota Amarilo [b,3], A. Samalan [b,4], K. Skovpen [b], G.A. Alves [c], E. Alves Coelho [c], F. Marujo da Silva [c], M. Barroso Ferreira Filho [d], E.M. Da Costa [d], D. De Jesus Damiao [d], B.C. Ferreira[d], S. Fonseca De Souza [d], L. Mundim [d], H. Nogima [d], J.P. Pinheiro [d], A. Santoro [d], M. Thiel [d], R. Gomes De Souza [d], T. De Andrade rangel Monteiro [d], A. Aleksandrov [e], R. Hadjiiska [e], P. Iaydjiev [e], M. Shopova [e], G. Sultanov [e], A. Dimitrov [f], L. Litov [f], B. Pavlov [f], P. Petkov [f], A. Petrov [f], E. Shumka [f], P. Cao[g], W. Diao[g], W. Gong[g], Q. Hou[g], H. Kou [g], Z.-A. Liu [g], J. Song[g], N. Wang[g], J. Zhao [g], S.J. Qian [h], C. Avila [i], D.A. Barbosa Trujillo [i], A. Cabrera [i], C.A. Florez [i], J.A. Reyes Vega[i], R.Aly [j,l,5], A. Radi [k,6], Y. Assran [l,7], I. Crotty[m], M.A. Mahmoud [m], L. Balleyguier[n], X. Chen[n], C. Combaret[n], G. Galbit[n], M. Gouzevitch [n], G. Grenier [n], I.B. Laktineh [n], A. Luciol[n], L. Mirabito [n], W. Tromeur[n], I. Bagaturia [o], O. Kemularia [o], I. Lomidze [o], Z. Tsamalaidze [o,8], V. Amoozegar[p], B. Boghrati [p], M. Ebrahimi [p], F. Esfandi [p], Y.Hosseini [p], M. Mohammadi Najafabadi [p], E. Zareian [p], M. Abbrescia [q,r], N. De Filippis [q,s], G. Iaselli [q,s], F. Loddo [q], G. Pugliese [q,s], D. Ramos [q], L. Benussi [t], S. Bianco [t], S. Meola [t,9], D. Piccolo [t], S. Buontempo [u], F. Carnevali [u,v], L. Lista [u,v,10], P. Paolucci [u,11], F. Fienga [w], A. Braghieri [x], P. Montagna [x,y], C. Riccardi [x,y], P. Salvini [x], P. Vitulo [x,y], T.J. Kim [z], E. Asilar [z], Y. Ryou [z], S. Choi [aa], B. Hong [aa], K.S. Lee [aa], J. Goh [ab], J. Shin [ab], Y. Lee [ac], I. Pedraza [ad], C. Uribe Estrada [ad], H. Castilla-Valdez [ae], R. Lopez-Fernandez [ae], A. Sánchez Hernández [ae], M. Ramírez García [af], D.L. Ramirez Guadarrama [af], M.A. Shah [af], E. Vazquez [af], N. Zaganidis[af], A. Ahmad [ag], M.I. Asghar [ag], H.R. Hoorani [ag], S. Muhammad[ag], J. Eysermans [ai],
on behalf of the CMS Collaboration

[a] *Vrije Universiteit Brussel, Brussel, Belgium*
[b] *Universiteit Gent, Gent, Belgium*
[c] *Centro Brasileiro de Pesquisas Fisicas, Rio de Janeiro, Brazil*
[d] *Universidade do Estado do Rio de Janeiro, Rio de Janeiro, Brazil*
[e] *Institute for Nuclear Research and Nuclear Energy, Bulgarian Academy of Sciences, Sofia, Bulgaria*
[f] *Faculty of Physics, University of Sofia, Sofia, Bulgaria*
[g] *Institute of High Energy Physics and University of the Chinese Academy of Sciences, Beijing, China*
[h] *School of Physics, Peking University, Beijing, China*
[i] *Universidad de Los Andes, Bogota, Colombia*
[j] *Physics Department, Faculty of science, Helwan University, Cairo, Egypt*
[k] *Department of Physics, Faculty of Science, Ain Shams University, Cairo, Egypt*
[l] *The British University in Egypt, Cairo, Egypt*
[m] *Center for High Energy Physics (CHEP-FU), Fayoum University, El-Fayoum, Egypt*
[n] *Institut de Physique des 2 Infinis de Lyon, Villeurbanne, France*
[o] *Georgian Technical University, Tbilisi, Georgia*
[p] *Institute for Research in Fundamental Sciences, Tehran, Iran*
[q] *INFN Sezione di Bari, Bari, Italy*
[r] *UniversitÃ di Bari, Bari, Italy*
[s] *Politecnico di Bari, Bari, Italy*
[t] *INFN Laboratori Nazionali di Frascati, Frascati, Italy*
[u] *INFN Sezione di Napoli, Napoli, Italy*
[v] *UniversitÃ di Napoli 'Federico II', Napoli, Italy*
[w] *Dipartimento di Ingegneria Elettrica e delle Tecnologie dell'Informazione - Università Degli Studi di Napoli Federico II, Napoli, Italy*
[x] *INFN Sezione di Pavia, Pavia, Italy*
[y] *UniversitÃ di Pavia, Pavia, Italy*
[z] *Hanyang University, Seoul, Korea*

Email addresses: mohammad.ahammad.ali@cern.ch (M. A. Ali), b.mahdy@cern.ch (B. El-Mahdy), fernando.enrique.neri.huerta@cern.ch (F.E. Neri Huerta)

[1] Also at Cairo University, Cairo, Egypt
[2] Also at Ghent University, Ghent, Belgium
[3] Now at UERJ, Rio de Janeiro, Brazil
[4] Now at PSI, Villigen, Switzerland
[5] Also at Academy of Scientific Research and Technology of the Arab Republic of Egypt, Egyptian Network of High Energy Physics, Cairo, Egypt
[6] Also at Sultan Qaboos University, Muscat, Oman
[7] Also at Suez University, Suez, Egypt
[8] Also at an institute or an international laboratory covered by a cooperation agreement with CERN
[9] Also at Università degli Studi Guglielmo Marconi, Roma, Italy
[10] Also at Scuola Superiore Meridionale, Università di Napoli 'Federico II', Napoli, Italy
[11] Also at CERN, European Organization for Nuclear Research, Geneva, Switzerland

[aa] Korea University, Seoul, Korea
[ab] Kyung Hee University, Department of Physics, Seoul, Korea
[ac] Sungkyunkwan University, Suwon, Korea
[ad] Benemerita Universidad Autonoma de Puebla, Puebla, Mexico
[ae] Centro de Investigacion y de Estudios Avanzados del IPN, Mexico City, Mexico
[af] Universidad Iberoamericana, Mexico City, Mexico
[ag] National Centre for Physics, Quaid-I-Azam University, Islamabad, Pakistan
[ah] University of Dundee, Dundee, Scotland
[ai] Massachusetts Institute of Technology, Cambridge, Massachusetts, USA

Abstract

In preparation for the Phase-II upgrade for the High-Luminosity LHC program, 72 improved Resistive Plate Chambers (iRPC) will be installed in the third and fourth endcap disks of the Compact Muon Solenoid detector during the annual technical stop 2024. This new generation of RPC detectors will operate in a low-angle momentum (extending RPC coverage from pseudorapidity $|\eta|$ = 1.9 to 2.4), in a high radiation environment, and will bring a better space and time resolution for this challenging region. To ensure proper performance, iRPC chambers undergo a series of quality control (QC) tests at each stage of the assembly chain. These tests include QC1 for the basic components, QC2 for chamber elements such as gaps and cooling, QC3 for evaluating the full chamber performance after production, which includes noise, efficiency, current, lastly QC4 for the final validation of the chambers. In this work we present the different QC stages and discuss test results for the newly built iRPCs at the assembly sites.

Keywords: Resistive Plate Chambers, Quality control, Performance.

1. CMS muon system

The Compact Muon Solenoid (CMS) detector [1] is a general-purpose apparatus that measures proton-proton and heavy-ion collisions at the Large Hadron Collider (LHC) at CERN. LHC has been operating at 13.6 TeV since the start of its third operational run, or Run 3, in July 2022. To enhance the sensitivity for new physics searches, a major upgrade of the LHC, called the High-Luminosity LHC [2], has been planned. This upgrade will increase the integrated luminosity tenfold compared to the original design values. The current "Phase-II" of LHC will end in 2026, followed by a shutdown for the High-Luminosity LHC upgrade, which will be completed by 2029.

The muon detector is placed in the outermost part of CMS, as high energy muons produced in LHC collisions can penetrate through the material of the detectors placed along their path from the interaction point. Muons, as electrons, interact weakly and electromagnetically, but due to their larger mass, their probability to generate electromagnetic showers is suppressed compared to electrons. This feature allows them to penetrate through the Electromagnetic (ECAL) and Hadronical (HCAL) calorimeters and the solenoid. The muon system in CMS comprises a cylindrical detector featuring a barrel section and two endcap sections. For the current phase, it employs three types of gaseous detectors, namely drift tubes (DTs), cathode strip chambers (CSCs), and resistive plate chambers (RPCs). For the phase-II, an upgrade in all types of detectors is taking place, and new detectors based on Gas Electron Multiplication (GEMs) technology are also being added.

2. improved Resistive Plate Chamber (iRPC)

The current RPC system consists of 480 chambers in the Barrel and 576 chambers in the Endcap, organized into 4 stations: RB1-4 (barrel) and RE1-4 in the endcap region. This implies that the RPC system is the only one that covers both the Endcap and Barrel locations. Two upgrade measures are planned for the RPC system. Although the existing RPC chambers can operate until the end of Phase-II, the Link Board (LB) system, which connects the front-end board (FEB) to the trigger processors, will be upgraded. Additionally, new detectors for the forward region (RE3/1 and RE4/1) are proposed [3]. Their future position can be observed in Fig.1.

New improved RPC chambers will be installed complementing the existing CSC chambers in that area. This upgrade is motivated by the need to increase the number of hits per muon track up to $|\eta| = 2.4$.

A significant improvement in the iRPC compared to the already installed RPCs is the reduced gap size of 1.4 mm (from 2 mm). Decreasing the gap size will lead to a faster avalanche formation and signal production, which lowers the charge threshold to less than 50 fC compared to 150 fC of traditional RPCs. Additionally, by reading signals from both ends of the printed circuit board (PCB) strips, the system will achieve impressive improvement in time resolution of 0.5 ns (compared to 1.5 ns in the RPCs). Spatial resolution will also see remarkable gains. In the radial direction, hit localisation precision will improve to 1.5 cm, a significant reduction from the 20 - 28 cm in the existing RPCs. Similarly, in the ϕ direction resolution will improve to 0.3 - 0.8 cm, compared to 0.8 - 1.9 cm in RPCs (strip pitch driven).

The iRPCs, illustrated in Fig. 2, feature a wedge-shaped design with radially oriented readout strips positioned between

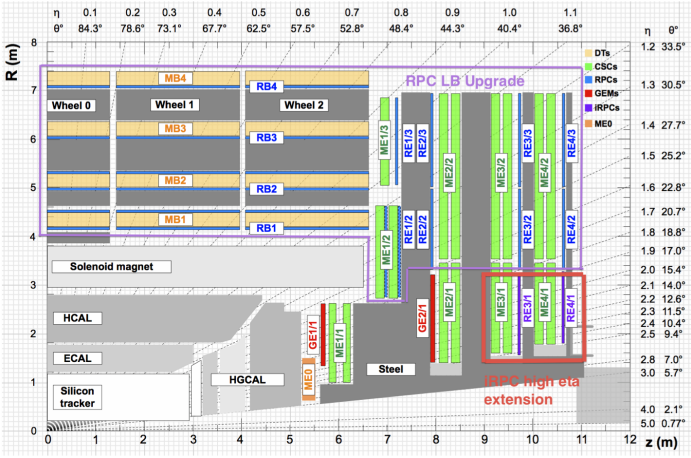

Figure 1: In red, the position of the two new RPC stations, RE3/1 and RE4/1, will cover the $|\eta| = 1.8$ to 2.4 region, complementing the already existing CSCs in that η range [2]. In purple, the current RPC detectors with upgrades in the LB system,. In the central part (left corner), the position of the calorimeters (ECAL and HCAL) is observed, in addition to a new detector for the update, the High-Granurality calorimeter (HGCAL).

the gaps. These chambers operate in avalanche mode and consist of two gaps, referred to as the top and bottom gaps. These gaps are formed by two High Pressure Laminate (HPL) electrodes coated with a thin graphite resistive layer, with the gas gap maintained by circular spacers between the HPL [4]. The current gas mixture used for RPC operation and testing is the standard CMS mixture: 95.2% $C_2H_2F_4$, responsible for generating primary ion-electron pairs; 4.5% iC_2H_{10}, which prevents photon feedback effects; and 0.3% SF_6, an electron quencher. The readout strips are integrated into a large trapezoidal PCB that is divided into two sections (PCB-left and -right) to fully cover the active area. Each PCB contains a total of 96 readout strips — 48 each in the left and right sections. Compared to the existing RPC system, the new readout scheme offers improved spatial resolution and reduces the number of electronic channels by 60%.

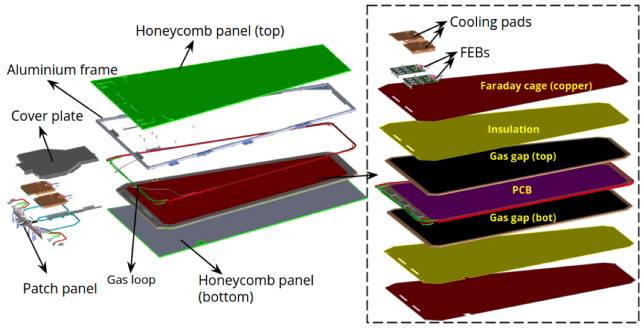

Figure 2: Illustrations of the internal structure of an iRPC detector. The detector consists of multiple layers, including two mylar sheets on top and bottom for insulation, two gaps and two PCBs, all enclosed within a Faraday cage.

All layers, including two insulation layers (mylar foils), two copper plates for the Faraday cage, and the gas connection circuits, are stacked inside a honeycomb panel-based box. To secure all layers in place, five aluminum brackets are mounted on four sides of the box. Additionally, the chamber is equipped with a fiber optic sensor to monitor environmental parameters such as temperature, pressure, and humidity. A patch panel is mounted on the aluminum frame to organize and hold the mechanics and cables in position. Two FEBs hosting the front-end electronics are connected directly to the PCBs, with two copper cooling pads placed on top of the FEBs to ensure temperature control. A cover plate is installed on the top of the chamber to protect the FEB connections and the cooling circuit.

3. Quality Control (QC) tests

3.1. QC1 for detector components

The initial stage of quality control (QC1) focuses on inspecting and validating essential components for detector assembly at procurement sites. Key components include HPL for gaps, detector electronics, strip PCBs, and copper cooling panels.

For iRPC FEBs, QC1 involves assessing each electronic module within the FEB, covering components like SCA, GBTx, power supplies, test points, etc. It verifies data transmission integrity, FEB firmware on FPGAs, and tests TDCs and ASICs. Performance is validated using injection boards simulating iRPC behavior.

The QC1 process for strip PCBs includes verifying electrical continuity of each strip, checking for breaks or interruptions, and minimizing crosstalk between neighboring strips [5]. Impedance values are confirmed, and crosstalk evaluations are redone after soldering ERNI connectors to prevent contact between strips.

3.2. QC2 for gas leak, spacer bonding and dark current

QC2 is a critical QC test conducted at the gap manufacturing facility in KODEL. This process includes gas leak tests, spacer bonding verification, and dark current scans to assess the performance and reliability of the gaps. Only the gaps that successfully pass these tests are approved for shipment to the chamber assembly sites.

Upon arrival at CERN's 904 laboratory or Ghent University for chamber assembly, a visual inspection is conducted and then QC2 tests are repeated. This preliminary evaluation is essential to ensure the integrity and functionality of the gaps before their integration into the chambers.

3.2.1. Gas leak and spacer bonding test

A gas leak test setup in the laboratory is used for QC procedures on gas gaps and chambers. It includes connection slots for Argon gas, input/output connections for gas gaps/chambers, a flow meter, and T connectors for gas distribution. A paraffin-filled bubbler serves as a safety measure against excess gas pressure, protecting against potential damage. A water column allows manual pressure measurement, with a pressure sensor and analog gauge for monitoring pressure. The pressure sensors are connected to a Pico ADC-24 data logger, which interfaces with a PC for data recording using Pico logger software.

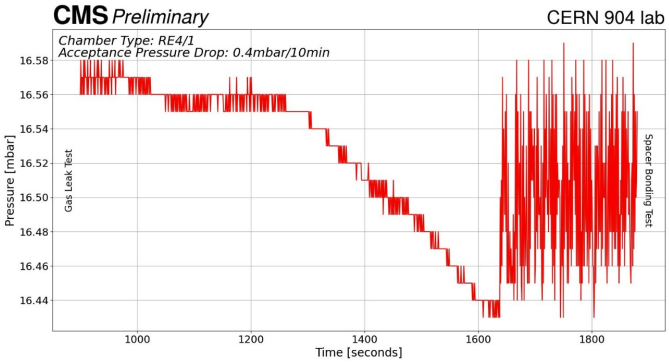

Figure 3: This plot shows the gas leak tightness and spacer bonding test for an iRPC gap at CERN 904 iRPC assembly site [6], after the gaps were manufactured in Korea and air shipped to CERN.

A gas leak test result is shown in Fig. 3, after filling the gap with Argon to a pressure of approximately 15 mbar, the gas leak test shows just a decrease of 0.15 mbar/10 min, well below the limit of 0.4 mbar/10 min. The spacer bonding test consists in laying a transparent template, with the spacers location marked on it, on top of the gap and applying pressure on each individual spacer. damaged spacer would easily be noticed as they would cause a high spike in pressure. In Fig. 3, this test is displayed between approximately 1600-1900s indicated smooth transitions between spacer components, ensuring good bonding quality. Overall, the detector demonstrated tight gas seals and secure spacer bonding, meeting the required standards for reliability. Therefore, the gap is able to progress to the next QC test stage.

3.2.2. Dark current test

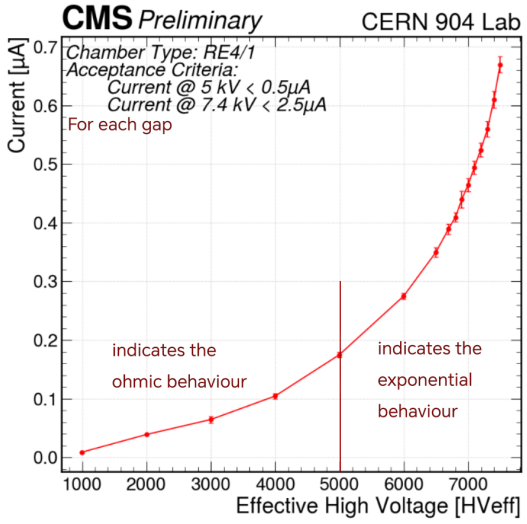

Figure 4: Dark current test results for a half chamber as a function of the effective high voltage (HV_{eff}) for an iRPC gap. In the linear ohmic region, the current increases proportionally with the voltage. The exponential rise in current begins around 6250 V, marking the transition to the exponential region.

For conducting dark current QC tests on gas gaps and chambers, a CAEN SY 1527LC multi-channel power supply system with integrated CAEN A1526 6-channel(15 kV) high voltage (HV) boards is utilized. The HV channels are managed through the visual interface of the power system.

The dark current test is completed to know if the appropriate electron avalanche is produced within the voltage range. The test done through 16 HV points to examine the Ohmic and exponential behavior in the gas gap. Figure 4 shows the result. The Ohmic behavior is clearly observed below 6.0 kV, followed by an exponential increase beyond this threshold. Based on this observation, 5.0 kV is chosen to assess the current in the Ohmic regime, while 7.4 kV serves as the reference for the exponential regime. For this QC stage, the maximum acceptable current is 0.5 μA at 5.0 kV and 2.5 μA at 7.4 kV.

In the case of dark current tests, particularly for the iRPC chambers, custom in-house software connected to the HV boards is employed, consistent with the software used during the RE4 RPC assembly.

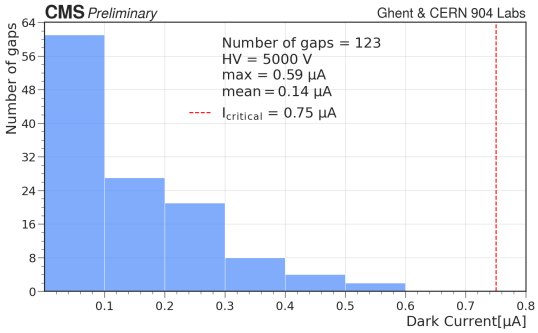

(a) Currents measured at 5000 V, highlighting the Ohmic behavior region. The maximum observed current reached 0.59 μA, with an average current of 0.14 μA, well within the acceptance criteria of 0.75 μA. Therefore, establishing a consistent performance evaluation.

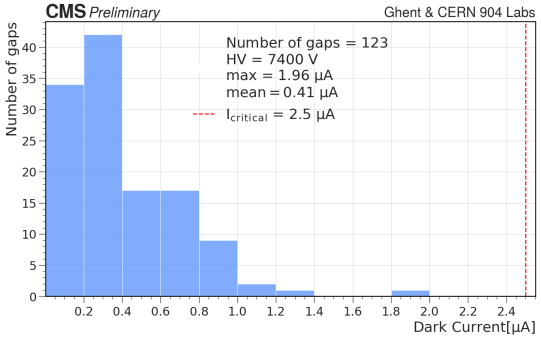

(b) Currents measured at 7400 V, illustrating the characteristics of the exponential region driven by the avalanche process. The maximum observed current was 1.96 μA, with an average current of 0.41 μA, conforming to the acceptance criteria of 2.5 μA, ensuring consistent evaluation of the system's performance.

Figure 5: Current measurements of iRPC production gaps tested at the assembly sites (CERN 904 and Ghent). All tests were performed under controlled laboratory conditions with an ambient temperature of 21°C, relative humidity of 55%, and gas humidity of 40%.

After that, concerning the study of performance of the assembled chamber in assembly sites, data from those plots are summarized for the aim of criteria validation. Figure 5 shows that these results align remarkably well with the acceptance criteria, establishing a consistent performance evaluation, while Fig. 5a (5b) examines the Ohmic (exponential) behavior.

After chamber assembly, a visual inspection ensures the integrity of external connections. Gas leak and dark current tests are repeated to validate gap condition. Leak tests are crucial due to assembly manipulations and the presence of multiple connections. Spacer bonding test is omitted in QC3 due to full chamber closure. Dark current tests were performed in QC3, by monitoring the current at 16 HV points, to ensure the desired behavior. Chambers exceeding 0.3 μA at 7.3 kV are rejected.

3.3. QC3 for chamber validation

In QC3 stage, three scintillator + SiPM (silicon photomultiplier) set in coincidence with an area of 30 x 40 cm^2. Chambers, equipped with 1 portable FEB on each side, were tested using cosmic muons. To exclude events caused by cosmic muon showers, an additional scintillator was placed near the chambers to serve as a veto detector.

Fig.6 shows the muon hit profile obtained with this setup configuration. The position of the hit takes into account the time difference from both sides of the readout strip.

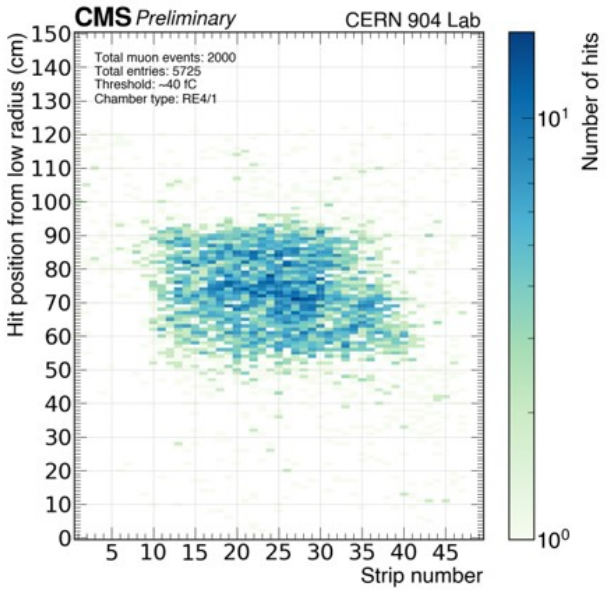

Figure 6: The plot shows a 3-dimensional reconstruction of muon hit positions for an iRPC chamber at a working point with a charge threshold of 40 fC.

One of the most critical quantity to measure during this stage is the efficiency, defined by the ratio of the number of detected muons to the total number of triggers. Figure 7 shows the efficiency measured for one tested chamber. A detected muon is considered as at least one hit within the scintillator projected area. Maximal efficiency reaches 99% for all four different readout windows.

Figure 8 shows the intrinsic noise distributions in Hz/cm^2 for one of the iRPC production chambers. This noise rate is measured by counting the number of hits in a variable time window. The ratio between the number of hits and the readout time gives the observed noise rate. This quantity is divided by the active detector area (strips area) to obtain the rate per square centimeter. 1 Hz/cm^2 is well within the expected range ($<$ 5 Hz/cm^2). This data was obtained with a corresponding charge threshold of $\approx$ 40 fC.

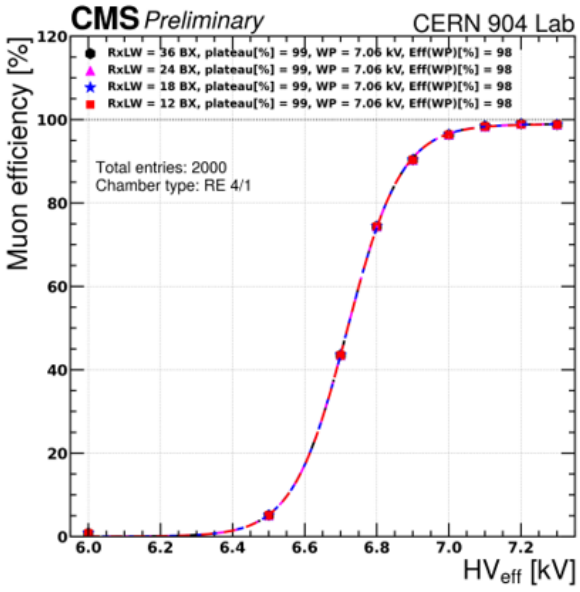

Figure 7: Cosmic muon detection efficiency versus effective high voltage (HV$_{eff}$). Efficiency peaks at 99%, with the working point at 95% (HV$_{knee}$) plus 150 V. The "RxLW"s in the legend are the receive latency windows, where "x" indicates how different of window size, in this case 36/24/18/12.

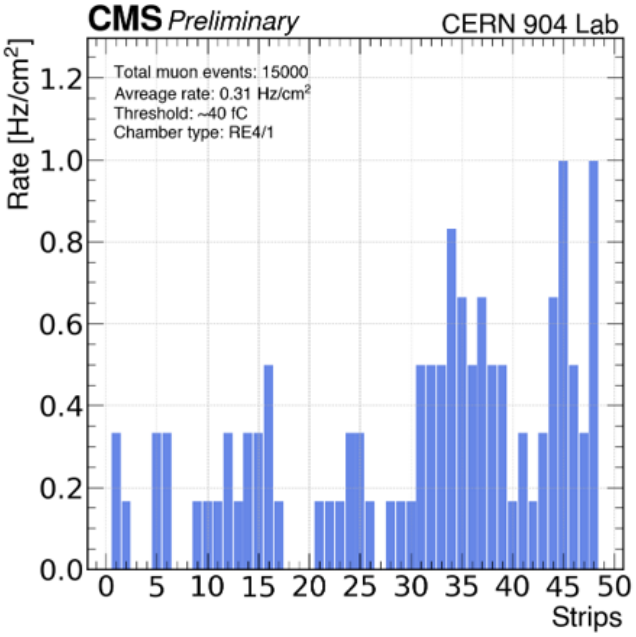

Figure 8: Noise plot of an iRPC at working point of 7.05 kV.

In an iRPC, strips in PCB varies due to the shape of detector, widths ranging 0.60 - 1.23 cm. At this QC stage, measurements are done from the high radius side of chamber, with strips around the scintillators measuring about 1 cm. This variation impacts spatial resolution. Figure 9 represents the cluster size, defined as the number of consecutive strips fired when a

muon crosses the detector. The total number of hits (two TDC data from each side of the same strip), recorded for each readout strip on the PCB, is shown in Fig. 10.

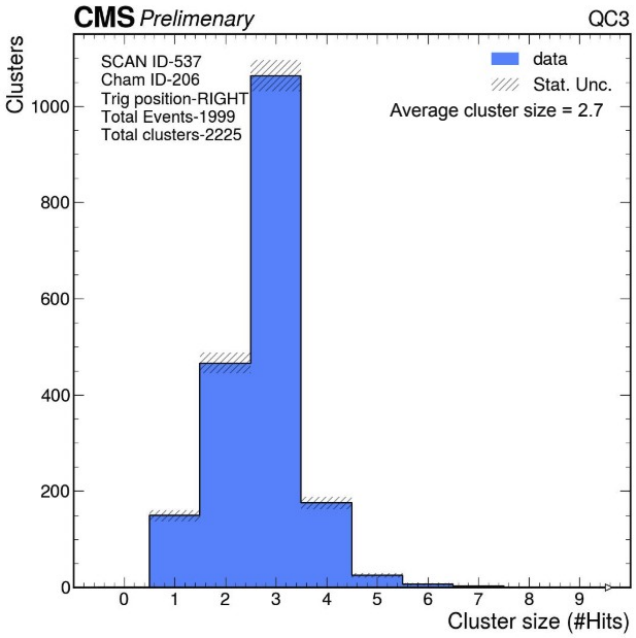

Figure 9: The plot shows the cluster size distribution at a working voltage of 7.05 kV for an iRPC detector.

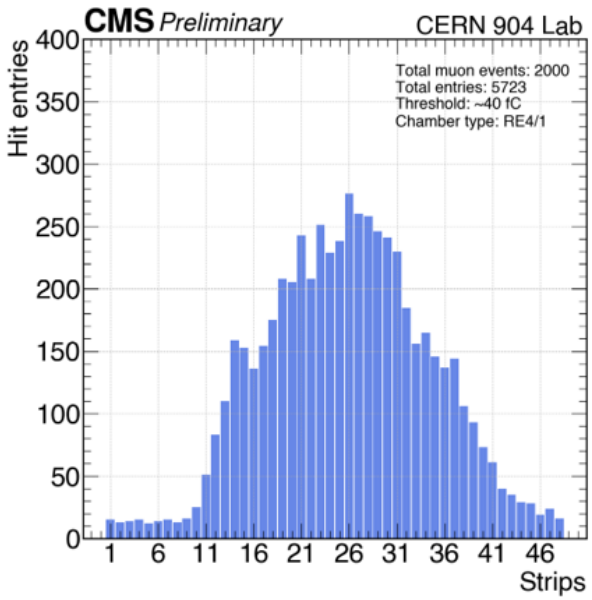

Figure 10: Strip hit profile recorded for each readout strip at a working point with high voltage around 7.05 kV.

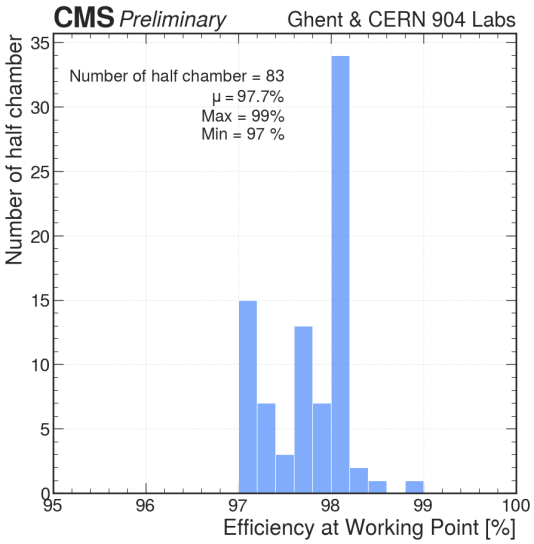

Figure 11: The histogram depicts the statistical distribution of Efficiency at Working Point values obtained from tests conducted using a portable FEB with charge threshold of ≃ 40 fC for both the left and right strip printed circuit boards.

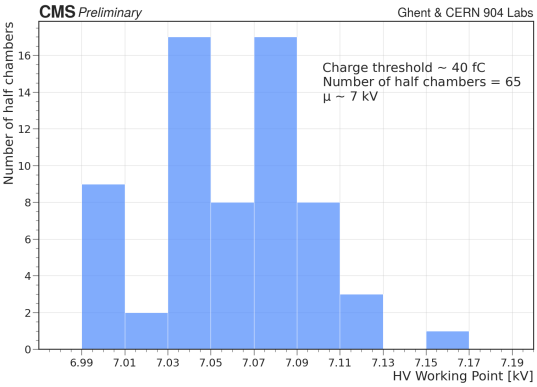

(a)

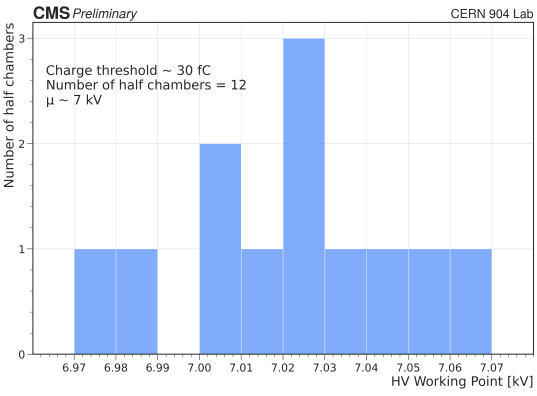

(b)

Figure 12: Dark current test result. The histograms depict the statistical distributions of HV Working Point (WP) values obtained for newly built iRPC chambers, from their cosmic quality control testing in assembly sites of (a) Ghent and CERN 904 and (b) CERN 904 only, conducted using a portable Front-End Board (FEBv23) with charge thresholds of (a) 40 fC and (b) 30 fC. The tests were done on both left and right strip printed circuit boards, testing each half of the chamber separately. It provides a visual representation of the distribution WP values, with a mean of 7 kV.

Highly occupied strips in the center ranging from from strip number 10 to number 38 of the plot correspond to the region from triple coincidence of three scintillators used as an external trigger. Referring to Fig. 11, chambers show high efficiency with mean value of 97.7% at working points shown in Fig. 12 with mean value of 7 kV.

3.4. QC4 for stability and verification

After chamber production and QC3 tests, all qualified chambers are transported to the CMS RPC lab at CERN, building 904. QC4 is the final chamber test, it involves three steps: QC4.1, QC4.2 and QC4.3.

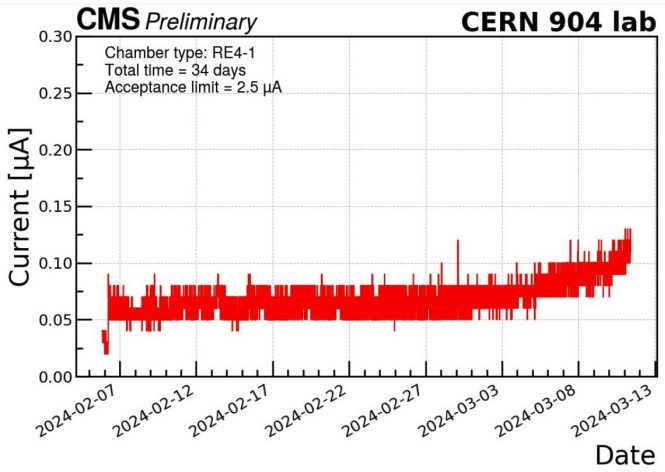

Figure 13: Results of the QC4.2 long-term stability chamber validation test. The current of one of the two HV layers of an iRPC production chamber at 7 kV over a period of more than a month is shown.

- QC4.1 – Cooling leak test, gas leak test, and dark current scan.
- QC4.2 – Long term HV stability, chambers remain at working point for a minimum period of a month. Currents, pressure, temperature and humidity are constantly being monitored. A chamber does not qualify in QC4.2 for installation in CMS if the current exceeds 2.5 μA. In Fig. 13, the down HV layer shows a stable trend, therefore it achieved a validation stamp from QC4.2 protocol.
- QC4.3 – Chamber tests with final FEBs. This test however, is currently ongoing and will be reported in a future publication.

The cosmic test bench has five scintillator + SiPM paddles for triggering and seven racks for iRPC chambers.

4. Conclusions

The production of the improved Resistive Plate Chambers (iRPCs) is in its final phase. A total of 62 chambers have been assembled to date, including 27 for the RE3/1 endcap station and 35 for RE4/1. The quality control procedures for iRPC assembly have been successfully validated for mass production. The results are uploaded to the CMS Construction Database for RPC data, which was adapted and validated to accommodate iRPC QC tests during the project.

The first two mass production chambers were installed on the CMS detector in the winter of 2023, the 70 remaining chambers will be installed in the year-end technical stop YETS24.

Acknowledgments

We would like to acknowledge the enduring support for the upgrade of the CMS detector and the supporting computing infrastructure provided by the following funding agencies: FWO (Belgium); CNPq, CAPES and FAPERJ (Brazil); MES and BNSF (Bulgaria); CERN; CAS, MoST, and NSFC (China); MINCIENCIAS (Colombia); CEA and CNRS/IN2P3 (France); SRNSFG (Georgia); IPM (Iran); INFN (Italy); MSIP and NRF (Republic of Korea); BUAP, CINVESTAV, CONACYT, LNS, SEP, and UASLP-FAI (Mexico); PAEC (Pakistan); DOE and NSF (USA).

References

[1] CMS Collaboration, *The CMS Experiment at the CERN LHC*, JINST 3 (2008) S08004. https://doi.org/10.1088/1748-0221/3/08/S08004.

[2] CMS Collaboration, *The Phase-2 Upgrade of the CMS Muon Detectors*, CERN-LHCC-2017-012, 2017. http://cds.cern.ch/record/2283189.

[3] CMS Collaboration, *Improved-RPC for the CMS muon system upgrade for the HL-LHC*, JINST 15 (2020) C11012. https://doi.org/10.1088/1748-0221/15/11/C11012.

[4] S. K. Park, *CMS Endcap RPC Gas Gap Production for Upgrade*, JINST 7 (2012) P11013. https://doi.org/10.22323/1.159.0032.

[5] A. Samalan, *Muon Detector Development for the CMS Phase-2 Upgrade and Muon Radiography Applications*, Ph.D. Thesis of Ghent University, CERN-THESIS-2024-025, 2024. https://cds.cern.ch/record/2894453.

[6] CMS Collaboration, *iRPC production gaps and chambers quality control*, CERN-CMS-DP-2024-104. https://cds.cern.ch/record/2916744.